The femtosecond field-emission camera, a device for continuous observation of the motion of individual adsorbed atoms and molecules

by G. M. McClelland
H. Heinzelmann
F. Watanabe

A new instrument, the femtosecond field-emission camera (FFEC), has been developed to continuously record the motion of single adsorbed atoms or molecules, with an ultimate achievable time resolution of 10^{-14} s. In the FFEC, the motion of an adsorbed species modulates a strong 10^{-5}-A field-emission current from a sharp tip. The emitted electrons are focused into a beam, which is swept electrostatically across a detector screen. The tip substrate can be imaged atomically by field ion microscopy. In this paper, the construction and operating principles of the FFEC are described in some detail, and previously

0018-8646/95/$3.00 © 1995 IBM

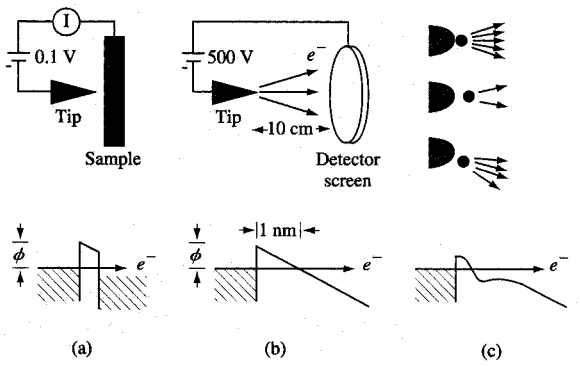

Figure 1

(a) Tunneling microscopy schematic and potential energy diagram. (b) Field-emission schematic and potential energy diagram. (c) Possible variation of the field-emission rate and direction as a function of the position of an adsorbed positive ion. Comparing (c) to (b) shows the effect of the atom on the field-emission potential. ϕ is the work function.

published experiments are reviewed. On a ⟨111⟩ W tip, single Cs atoms are observed to jump between sites instantaneously within the 2-ps instrumental resolution. Individual copper phthalocyanine molecules are observed vibrating with respect to the substrate with a period of ≃10 ps. The time resolution of the FFEC is limited principally by the time-of-flight spread of the electrons between the tip and the deflecting field.

Introduction

The idea that physical and chemical processes arise from atomic motion was well accepted a century ago and was put on a firm theoretical foundation in the 1930s with the advent of quantum mechanics. As early as 1936, the atomic trajectories of a reactive collision were computed numerically (using hand calculators!) on a theoretically derived electronic potential energy surface [1].

Experimental observations of atomic dynamics have lagged behind the early conceptual advances of theory. Perhaps the most specific experiment that can be envisioned is to observe continuously the trajectories of the atoms in a single physical event, such as the hopping of an adsorbed atom or the making or breaking of a chemical bond. But until fairly recently, observations of chemical reactions gave only a rate constant as a function of temperature, data which provide the energy and entropy of the activation barrier surmounted as the reactant molecules convert to products. Around 1960, this chemical kinetics approach was enhanced by the application of molecular beam and spectroscopic (including laser) techniques to measure the rates of single-collision processes to and from individual quantum states [2]. The energy, angle, and velocity distributions observed in these state-to-state dynamics measurements contain much information about the atomic trajectories during a collision, but interpreting the data is often not straightforward.

Time-resolved observations of atomic motion became possible only with the development of subpicosecond lasers, whose pulse duration is shorter than the vibrational periods setting the time scale for the evolution of atomic trajectories. Such lasers are employed in pump-probe experiments, in which an ensemble of molecules is promoted coherently to an electronically excited state, and the subsequent motion is probed by a second, delayed pulse [3]. By observing the evolution of a spectroscopic signal as a function of the delay, the time dependence of the atomic geometry can be recorded. This powerful technique can be extended to chemical reactions [4]. However, optical techniques cannot continuously observe the motion of single atoms, molecules, or interacting atoms and molecules, because the techniques are insufficiently sensitive, and because optical probes drastically perturb the atomic motion by causing a transition between potential energy surfaces. (However, Dhar, Fourkas, and Nelson [5] have obtained a complete set of pump-probe data in a single laser shot by exciting a spatially extended sample in which the delay between the counterpropagating pump and probe beams depends on the position of a molecule within the sample.)

Compared to an optical process, an electron-scattering process is better suited to continuously probe atomic positions, because the scattering of the low-mass electron has a relatively weak effect on the motion of an atom, and can occur without altering the electronic state. Electron diffraction from a pulsed electron gun following laser pumping has been advocated as a method for probing fast dynamics [6], but a conventional electron gun flux is too weak and the scattering probability too small to continuously monitor a single molecule. A very high-density source of electrons is a scanning tunneling microscope (STM) tip [**Figure 1(a)**]. The tunneling electrons perturb the sample only weakly; an electron has only a ≃1% chance of causing a vibrational transition of an adsorbate, and a selection rule favors only single-quantum vibrational transitions [7]. The STM provides atomic resolution and indeed is capable of very high-bandwidth measurements, because the tunneling process is fast [8], and the STM wiring can be miniaturized for fast electronic response. Unfortunately, because the STM tunneling current is measured by conventional analog electronic methods, the noise level is very high, much higher than

the lower limit set by shot noise. Real-time picosecond measurements are not feasible, although fast optical [9] and electronic sampling [10] (essentially pump-probe) measurements averaging over many pulses have been reported. Similarly, electrostatic force microscopes can achieve picosecond resolution by fast electronic gating of the tip potential [11].

To avoid the high noise of the STM tunneling configuration, we instead use field emission (FE) [12] to observe ultrafast single atom and molecule dynamics. (The topografiner [13], an early low-resolution version of the STM, in fact developed out of research in FE.) The FE technique [**Figure 1(b)**], which was developed in the 1930s, is a tunneling technique similar to STM, except that in FEM the negatively biased ($\simeq -500$-V) tip, which acts as a sample, is centimeters from a grounded screen, rather than angstroms from a surface. Despite this large separation, the sharp tip radius maintains a high field at the tip and a narrow tunneling barrier [Figure 1(b)]. Electrons tunneling from the tip are emitted into vacuum and accelerated onto the detection screen. The electrons are accelerated radially out from the spherical tip, so that the distribution of the electrons on the screen forms an image of the spatial distribution of emission intensity. Because the electrons strike the screen at high energy, they can be detected with nearly 100% efficiency, so the shot noise limit can be achieved.

Our interest in FE to probe ultrafast dynamics was prompted by Fink's discovery that 10^{-5} A of current can be emitted from a three-atom terminating plane of an ultrasharp ⟨111⟩-oriented tungsten tip [14]. These tips were originally fabricated [15] as high-resolution tips for STM, an application several groups have pursued [16–18]. As electron point sources, these and other [19, 20] carefully sharpened tips have been used for electron holography [21], high-resolution surface scattering [14], scanned lithography [22], projection microscopy [23], and scanning electron microscopy [22, 24]. Their usefulness for ultrafast dynamics experiments arises from the fact that 10^{-5} A corresponds to an emission rate of 6×10^{13} electrons per second, a rate much faster than vibrational periods of heavy surface atoms. It is well known that FE can be significantly altered by the presence of a single atom on a surface [25]. Thus, ultrasharp FE tips provide a substrate for observing ultrafast dynamics by a scheme illustrated in **Figure 1(c)**. As the atom changes position, the electron emission rate is modified by the changing shape of the tunneling barrier. Previously, millisecond FE fluctuations from the motion of individual molecules have been observed [26–29], and diffusion rates of ensembles of molecules have been determined by observing millisecond FE fluctuations from tip regions measuring ≈20 nm across [30].

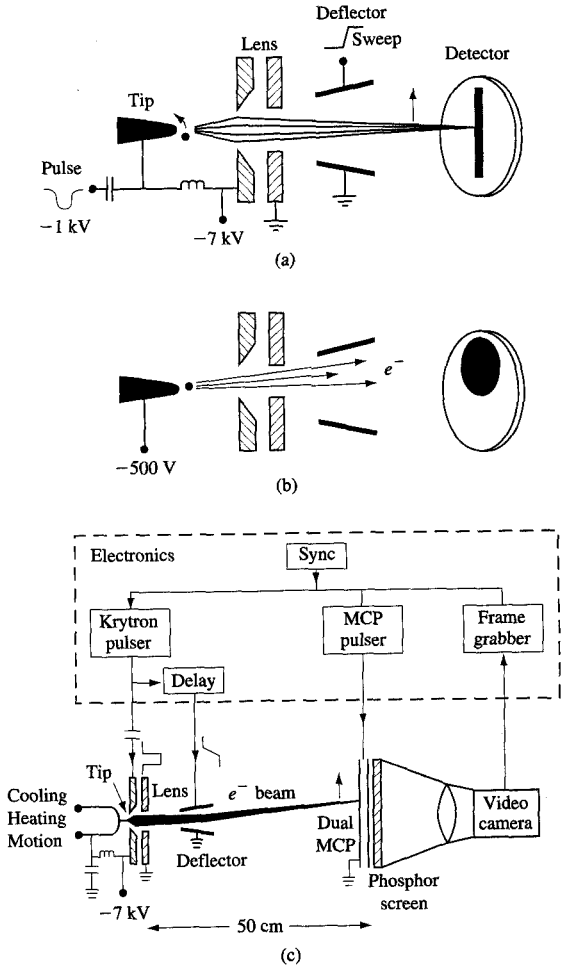

Figure 2

Femtosecond field-emission camera. (a) Time-resolving mode, in which the electrons are focused and swept across the detector screen. (b) Imaging mode, in which the emitted electrons are projected onto the detector to spatially resolve their emission point on the tip (field-emission microscopy). For FIM imaging, the tip voltage is made positive. (c) More detailed diagram of the instrument, shown in time-resolving mode. From [32] and [36], reproduced with permission; © AAAS.

To record the varying emission rate at the picosecond and subpicosecond time scale, we have developed the femtosecond field-emission camera (FFEC) [31, 32]. In this instrument, the emitted electrons are focused into a narrow beam and electrostatically deflected across a sensitive detector screen [**Figure 2(a)**]. The principle is adopted from the electro-optic streak camera [33], replacing the photocathode with the tip as an electron source. The spatial density of the detected electrons as a function of

position at the screen records the FE rate as a function of time. By using small optics, sharp focusing, and high sweep rates, 10^{-14}-s resolution is achievable. Related techniques include a nanosecond sweeping method to record the ion production rate of a liquid metal ion source [34] and an electron optical gating technique for probing the statistics of FE [35]. As explained more fully below, the FFEC can also be used in an imaging mode [**Figure (2b)**].

We have used the FFEC to observe the jumping of adsorbed Cs atoms [32] and the vibration of adsorbed copper phthalocyanine molecules [36]. This previously published work is reviewed here, and a detailed description of the instrument construction, operating principles, and capabilities is presented.

Femtosecond field-emission camera

Figure 2(c) is a schematic of the FFEC, which is housed in a bakeable stainless steel vacuum chamber to achieve a base pressure of $\simeq 2 \times 10^{-11}$ torr. To cancel the earth's magnetic field, which would distort the electron trajectories, electromagnets are formed from loops of wire around the chamber.

A tungsten tip of ≃50 nm radius is prepared by electrochemical etching (using a drop-off technique [37]) and spot-welded to a tungsten wire loop for heating. The loop is fixed to a manipulator with two rotational and three translational degrees of freedom. A sapphire rod provides 10-kV electrical insulation for field ion microscopy (FIM), while simultaneously anchoring the manipulator to a liquid nitrogen cold-finger, which also provides fast cryopumping. The tip is aligned about 6 mm behind a lens modeled after an FE scanning electron microscope design [38]. The lens element spacing is 3 mm, and the entrance aperture diameter is 0.08 cm.

About 4 cm past the lens are positioned two 2.5-cm-long deflection electrodes, separated by 0.5 cm at their entrance, and tilted in line with the tip to present the least cross section in the projection microscopy mode (see below). The deflected electrons travel an additional 50 cm before striking a sensitive detector assembled from two sequential microchannel plates (MCP) mounted in a chevron configuration followed by a phosphor screen[1]. The screen luminescence is focused onto a video detector, either a silicon intensifier target vidicon or a charge-coupled device, and recorded by a video frame grabber.

A krytron device (Fastpulse Technology Corporation Model 8612)[2] generates a 1-ns-rise-time 1–4-kV pulse, which is shaped by a low-pass filter to generate the deflection sweeping voltage. To restrict the field emission to the duration of the sweep, the tip field is gated by directing a fraction of the positive pulse through a resistive network to the first lens element, which acts as a counterelectrode to the tip. The background from spurious electrons (from, e.g., the lens) is reduced by gating on the MCP for only 100 ns with a pulse generator (Directed Energy Company Model SVX-800).[3]

To calibrate the time base, the FFEC is used as an oscilloscope by applying a waveform to a second set of deflection plates oriented orthogonally to the sweeping set. (This second set is normally held at a constant voltage to offset the beam position.) For slow scanning speeds, a 2.5-GHz sine wave is applied to the plates. For fast speeds, a portion of the krytron pulse is applied to the calibrating plates, and the shift in waveform position is observed as the time delay between the sweeping and calibrating signals is varied by adjusting a cable length.

Because of the angle at which the deflecting plates are installed, when the lens is turned off, the FFEC can be used as a standard field ion microscope [37] or field-emission microscope [12] [Figure 2(b)], in which the electrons or ions are simply projected in a straight line toward the detector. Unfortunately, the observable angular range is limited by the long distance between the tip and the detector, a problem improved by applying an underfocusing voltage to the lens to partially converge the ions or electrons.

• *Forming ultrasharp tips*

The fine spatial resolution of the STM arises in part from ultrafine mechanical motion. In the FFEC, the fine resolution arises strictly from the sharpness of the tip.

To form an ultrasharp atomically characterized sample surface, we apply Fink's sequence [14, 15] of standard FIM processing steps to a ⟨111⟩-oriented tungsten tip. After the chamber has been evacuated and baked, the tip is first flashed to 1100 K to remove gross contamination. While the tip is observed by FIM in 5×10^{-5} torr He imaging gas, the tip is field-evaporated at ≃7 kV to a near-spherical shape showing the atomic lattice. Flashing the tip to 1100 K converts it to a more thermodynamically stable sharp three-sided pyramid shape, each side a (211) plane. Further field evaporation modifies the very apex of the tip. For the Cs experiments [32], we left the tip as a trimer of adjacent atoms of a (111) plane, but it is possible to form a tip terminating in a single atom [14, 15]. The {211} planes make a rather large (70.5°) angle with the tip axis; other methods produce narrower tip angles [19, 20].

Repeated "sharpening" to produce a localized point on the tip actually dulls the overall radius of the tip. After about six treatments, the voltage required to generate the FE field becomes so high that the required lens focusing voltage (about seven times higher) may cause a discharge.

[1] Dual MCP and phosphor screen assembly manufactured by Galileo Corporation, Sturbridge, MA.
[2] Fastpulse Technology Corporation, Englewood, NJ.
[3] Directed Energy Company, Fort Collins, CO.

At this point, the tip radius is sputtered smaller by field-emitting into 10^{-4} torr Ne, which is electron-impact ionized and accelerated toward the tip by the FE voltage [39]. (Any process which removes tip atoms at a rate independent of the local curvature tends to sharpen the tip.) After several applications, this treatment itself fails to sharpen the tip. At this point, oxygen etching at 1700 K almost always restores the tip [40]. Using these methods, we have experimented for a year on a single W sample without removing it from its holder. Installing a new tip in the manipulator has been necessary only after a lens discharge. (Unfortunately, a lens discharge seems to dull the tip drastically even when the tip has been withdrawn from the lens to confine the discharge to the lens interior. This effect, believed to be due to capacitative and/or inductive coupling, prevents conditioning the lens by a controlled discharge to allow a higher voltage to be sustained.)

Jumping of Cs atoms on a tungsten tip

In our first FFEC experiments, we observed the jumping of Cs atoms adsorbed on a tungsten tip [32]. A single Cs atom strongly affects the field emission because the electropositive atom becomes positively charged upon adsorption, forming a dipole which lowers the effective work function [see Figure 1(c)]. A more detailed understanding of the atom's effect on FE requires a careful analysis of the effect of changes in the atomic orbitals [41].

After formation of a ⟨111⟩ tungsten tip terminated by a trimer, the tip is monitored by observing a video display of a low-current (10^{-12}-A) field-emission image representing a region 20 Å across. The scale of these images can be calibrated from the FIM image of the bare tip, which has the same magnification and (unlike FE) shows the atomic lattice. While the tip is held at 90 K to freeze out diffusion, Cs is evaporated from a gettering source (SAES Company)[4] at a very low flux chosen to land a Cs atom on or near the observed area at ≈60-s intervals. The adsorbed atom increases the local FE intensity by a factor of ≈5. Because the Cs atom is adsorbed with a large positive charge, it can be field-desorbed by applying a positive voltage to generate a 4-V/nm field [25]. The tungsten field evaporation threshold is 50 V/nm [37], so the tungsten surface is unchanged during Cs removal. Atoms which land near the image edge are field-desorbed until an atom lands near the center of the image.

To observe atom jumping, the emission current is raised to $\approx 5 \times 10^{-6}$ A by pulsing the lens to higher voltage. This increased current heats the Cs atom by two mechanisms. The electronic temperature at the tip surface is raised by strong FE, because the average energy of emitted electrons is lower than that of the electrons arriving at the surface by conduction. This Nottingham effect [42] raises the vibrational temperature of the lattice and the adsorbed atom as the vibrations come into equilibrium with the electrons. Another heating mechanism is inelastic electron tunneling, in which an electron loses energy to a Cs or W atom vibration [7, 28].

To observe the jumping of a selected Cs atom, a series of alternating sweeping and imaging experiments are performed at 2-s intervals while the manipulator is held at 90 K. The low-current imaging experiments [the mode illustrated in Figure 2(b), lens voltage reduced or off] display the position of the atom after it has cooled following the previous sweep, in which jumping may occur. In the sweeping experiments, we adjust the tip voltage pulse (and with it the proportional lens-focusing voltage) to achieve an emission current high enough to cause the Cs atom to jump typically somewhat less than once per sweep. Based on an estimated barrier of 0.5 eV for Cs atom diffusion, this jumping rate corresponds to a temperature of ≈800 K. At higher emission currents, several jumps per sweep are sometimes observed.

From a series of experiments on a single Cs atom, **Figure 3** shows sweeps 1, 6, 7, and 8, and the images taken after each sweep [32]. During sweep 6, no jumping occurred. The bell shape is due simply to the limited rate at which the lens voltage can be changed to pulse the tip field. (The requirements of high voltage, cryogenic insulation, and movability make it difficult to control the tip potential with a high electrical bandwidth.) The data points of sweep 6 are fit by a solid line, which is reproduced with the other sweep data as a reference.

Sweeps 1, 7, and 8 each show an abrupt transition, indicating a sudden jump of a Cs atom on the surface. The width of the transition is limited by imperfect focusing of the electron beam. The Cs atom appears to occupy one of two sites at the ends of the sweep. One site, called H here, gives high FE because the Cs atom is near the center sharp portion of the tip. Another site, called L, is at the upper left-hand portion of the tip. In sweep 1, the atom moves from the L to the H position, while between sweeps 1 and 6 it moves back to the L position. During sweep 7 the atom again moves from L to H, while during sweep 8, the atom moves back to the L position, giving smaller FE. Although the jumping of the Cs atom is a statistical process, the jump occurs at roughly the same point in sweeps 1 and 7, when the FE is strong enough to heat the atom sufficiently to jump over the barrier between sites.

The two FIM images of Figure 3 demonstrate that the underlying atomic geometry of the tungsten tip is unchanged during the series of sweeps.

In the experiments just described, the emission direction of an electron leaving the tip indicates the location of its emission, but this information is lost as all electrons are focused to a spot for sweeping. Focusing in the direction

[4] SAES Company, Milan, Italy.

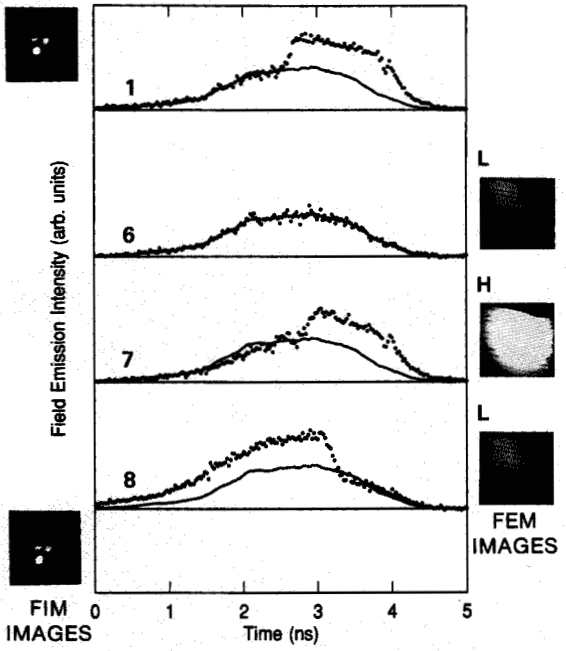

Figure 3

Series of sweeping and imaging experiments documenting the jumping of a single Cs atom between two adsorption sites on a tungsten tip. The numbered plots present the time-resolved field-emission intensity for four of eight consecutive sweeps. The time axis is referenced to the tip voltage pulse, and a smoothed sweep 6 is superimposed on all plots. The field-emission images to the right are recorded after each sweep. At the same magnification, FIM images taken before and after the field-emission measurements of the three W atoms (spacing, 4.5 Å) of the apex layer of the tip are presented at the upper and lower left, respectively. The upper left atom image is partially blocked by a deflection electrode, and the equilateral geometry of the three atoms is distorted by the focusing optics. From [32], reproduced with permission.

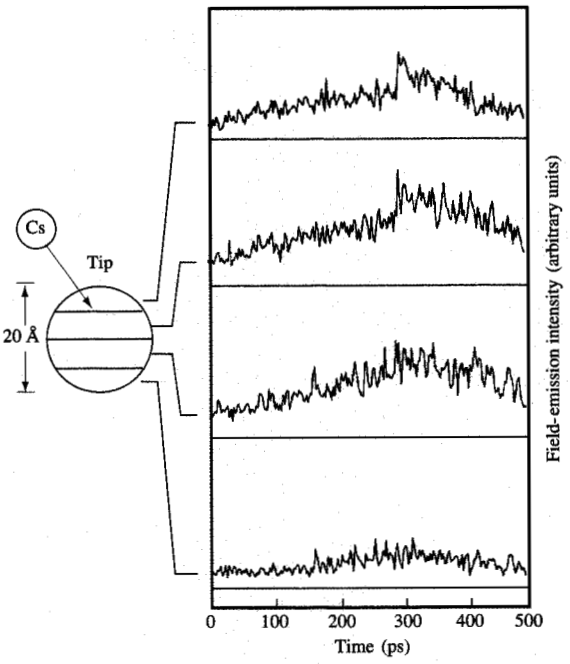

Figure 4

Simultaneous temporal and one-dimensional spatial resolution of field emission, showing the jumping of a single Cs atom. The four plots, recorded simultaneously, present field emission from four adjacent regions of the tip. Consecutive data points, separated by 2 ps, are connected by a straight line. The schematic indicates a possible motion of the adsorbed Cs atom consistent with the field emission. From [32], reproduced with permission.

parallel to the sweep direction is obviously essential for good time resolution, but there is no need to focus along the perpendicular direction. By using the astigmatic properties of the imperfect lens to focus sharply only along the sweep direction, the spatial distribution of electrons perpendicular to the sweep direction can be retained.

Employing this scheme, **Figure 4** shows a single trace at faster sweep speed, in which the detector signal has been resolved into four adjacent rows of detector pixels, representing four adjacent regions on the tip [32]. The two top traces show an abrupt rise in the FE within the 2-ps pixel length, while the lower traces show no such abrupt change. These results (which were obtained on a clean tip but one not imaged by FIM) are consistent with a Cs atom jumping from outside the observed region onto the top portion of the tip, as diagrammed in Figure 4. In this sweep, the overall peak shape arises from the occlusion of the beam at the beginning and end of the trace by the deflection plates.

Observing the vibration of a single molecule

Although the time resolution of our atomic jumping experiments is a vast improvement over previous continuous single-atom observations, within our time resolution, the jumping transition is nevertheless instantaneous. To truly follow dynamics, a motion with a characteristic signature within the time resolution of our instrument is required. For this purpose, we chose the vibrational motion of a very large and heavy molecule. Copper phthalocyanine (CuPc) has a molecular weight of 576 and is thermally stable to well above its sublimation temperature. (CuPc was the subject of the first STM observation of the internal structure of a molecule in ultrahigh vacuum [43].) It has long been known that single CuPc molecules can enhance FE by a factor of ≃100

[27, 44, 45], apparently by a mechanism in which electrons tunnel out of the molecule into a field enhanced by the protrusion of the molecule from the surface [27, 44]. The emitted electron is replaced by one tunneled from the surface. The delocalized π electronic states of the molecule may aid in the "conduction" of electrons through the molecule.

The motion of any species in the FFEC is strongly influenced by the ≈10-V/nm field at the tip, which interacts with any molecular dipoles or polarizabilities. Due to its delocalized π-bonded electronic structure, CuPc is most polarizable in a direction parallel to its plane. The polarization interaction favors by 2 eV a molecular orientation perpendicular to the tip surface (parallel to the field) over one parallel to the tip surface (**Figure 5**) [36]. From the effective force constant for this motion and the moment of inertia for the pivoting vibration (libration) about the end of the molecule, a vibrational period of ≈10 ps is expected [36]. Of course, other binding interactions would tend to favor CuPc lying flat along the surface, an effect which might further reduce the frequency. Other adsorption geometries, for example a molecule "teetering" on a step edge [26], might yield similarly low frequencies.

For the CuPc experiments, FIM was not used to characterize the tip, but field evaporation and thermal annealing were employed to form a tip apex ≈2 nm across [36]. As for the Cs experiments, the tip was cooled to 90 K to stop thermal motion, and the low-current field-emission image was observed while a very low flux of CuPc effused toward the tip from a heated evaporation boat. On a clean tip, the first few landing molecules each abruptly decreased the FE, presumably by increasing the local work function. (Unlike Cs atoms, CuPc molecules cannot be neatly removed from the tip by field desorption.) Eventually a landing molecule caused a large (factor of >50) increase in FE. Such a molecule is likely physisorbed on previously landed chemisorbed molecules.

After a strongly emitting molecule had adsorbed, a series of alternating imaging and sweeping experiments was performed. Within about 20 sweeps after the original increase in brightness, the emission intensity decreased during a sweep, presumably due to desorption or decomposition of the molecule. To maximize the chance of observing molecular dynamics, only the first three sweeps after a sudden increase in FE were analyzed.

Of a total of 270 sweeps analyzed, 13 showed a significant sinusoidal FE oscillation [36]. (The term *significant* is defined precisely below.) Data from three such sweeps are displayed in **Figure 6**. In addition to the FE [$P_i(t)$ is the field emission during the ith sweep] vs. time, the autocorrelation function (ACF) and power spectrum of the FE are displayed. (The analysis is described in detail in Reference [36].) The sweep of Figure 6(a) contains an abrupt decrease in the FE, corresponding

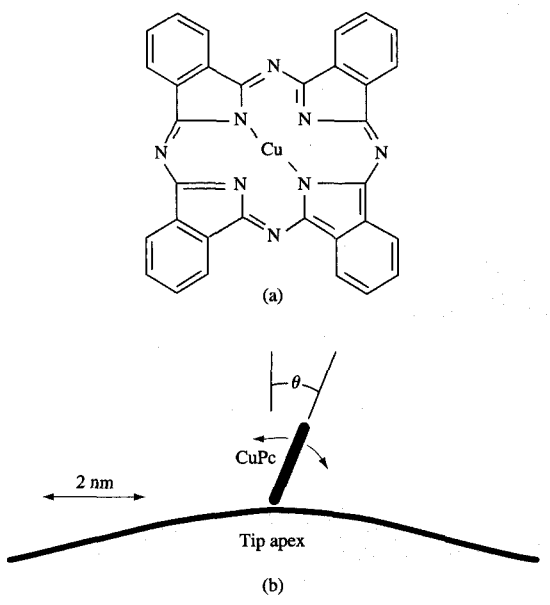

Figure 5

(a) The copper phthalocyanine (CuPc) molecule. (b) Schematic of a CuPc molecule (viewed edgewise) adsorbed on the end of a tungsten tip, showing a possible observed vibrational motion. The perpendicular orientation is energetically favored by high electric fields. From [36], reproduced with permission; © AAAS.

to an abrupt motion, which might generate a large amplitude vibration. A periodic but noisy component can indeed be distinguished in the FE signal, and is evident in the ACF and power spectrum.

Similar periodic components were observed over full traces and over portions of traces, for example Figures 6(b) and 6(c), arising from FE-induced heating of the CuPc vibration. As indicated by the sinusoids in Figure 6, in some cases the periodic variation is as large as a factor of 2 variation in FE.

Although the time-domain results are of primary interest, the significance of the oscillations is more readily judged by their frequency spectra. Are the sweeps which show periodic components simply those in which the noise (principally electron-counting shot noise) happens to peak at a particular frequency? A numerical simulation of the noise sources answers this question [36]. In addition to electron-beam shot noise, the MCP gain statistics, the measured screen imaging slit function, and the overall trace shape were taken into account. In addition, the possibility was included of observing an oscillating component due to the approximately periodic motion of

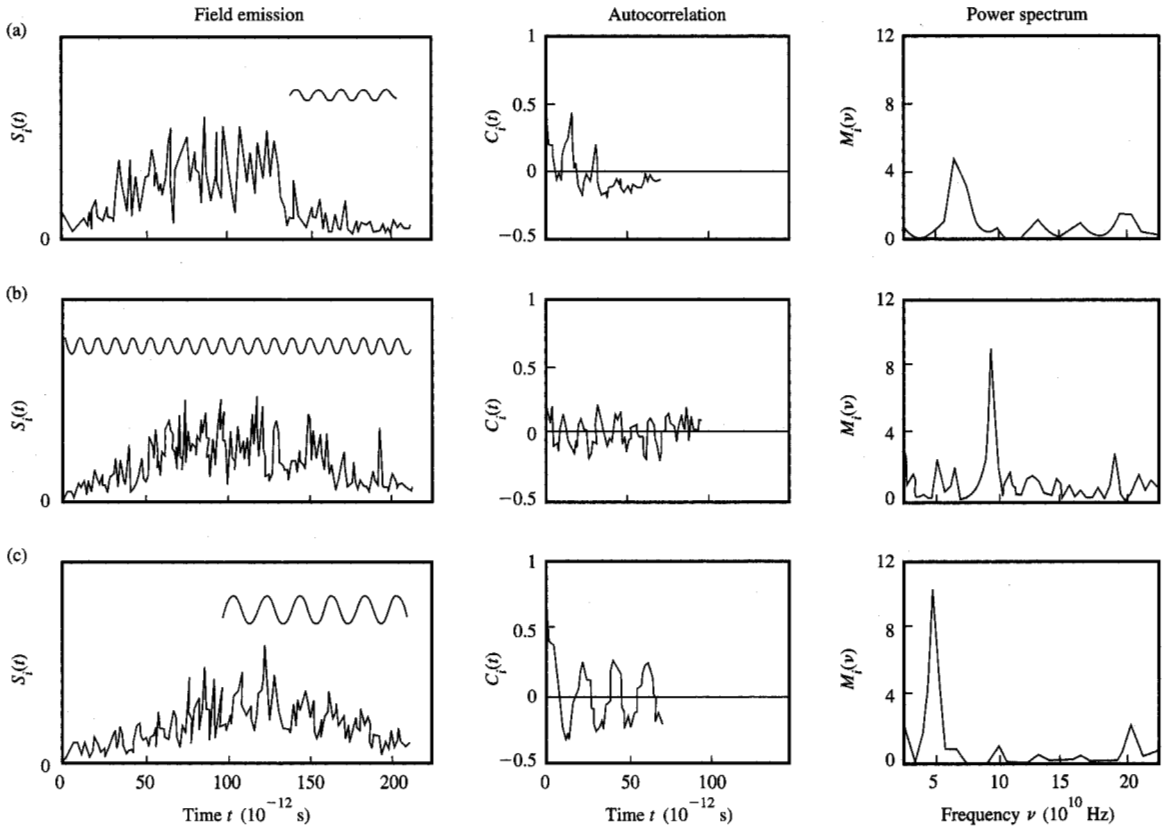

Figure 6

Three individual time records showing sinusoidal field-emission oscillations attributed to molecular vibration. The first column plots the field emission, $S_i(t)$, during the ith sweep vs. time. Over the time interval in which a sinusoidal oscillation was detected, the smooth sinusoid above the data represents the amplitude of the observed oscillation with the noise removed. The second and third columns present the autocorrelation function and the power spectrum. In (a), an oscillation is observed after an abrupt change in field emission; in (b), the oscillation continues through most of the trace; and in (c), the oscillation occurs during the last half of the trace. From [36], reproduced with permission; © AAAS.

a randomly flip-flopping molecule. However, the exact details of the model have little effect, because the predicted noise spectrum is very nearly that of white noise. Using this model, the probability $P(M)$ of observing the power spectrum peaked as high as some particular value M arising from noise alone can be computed. For a peak height M for which the model predicts only a single observed peak over all 270 analyzed sweeps, we instead found 13 sweeps peaked at this height, indicating that the signal is indeed real. To check the validity of our noise model, 100 sweeps from a clean tip were analyzed. The statistical distribution of the peak heights observed was in exact agreement with the noise model.

The 13 frequencies observed are rather evenly distributed within the experimentally observable 5×10^{10} to 20×10^{10}-Hz range [36]. This distribution could arise from varying orientations of the adsorbed molecules, from occupation of varying binding sites, varying local field strengths across the tip, and the varying position of surrounding molecules or fragments. Between sweeps the frequency is expected to change as the molecule occupies a new local potential minimum in the changing electric field.

Although noise can be ruled out as the source of the FE oscillations, the possibility cannot be excluded that the vibrations are those of oscillating fragments or clusters

[44], although the latter possibility is inconsistent with the sudden FE increase observed during deposition, which is presumably due to the landing of a single molecule.

Instrumental performance

- *Time resolution*

As in STM, the time resolution of FE is limited fundamentally by the $\simeq 10^{-15}$-s distribution of transit times through the tunneling barrier [8]. The FFEC is capable of resolving the electron deflection quite accurately, because the beam focuses tightly on the detector screen. Because of the extremely small size of the electron source, coma aberration is negligible, and the principal aberrations limiting the spot size are spherical and chromatic [38]. Chromatic aberration is small because of the small energy spread of the emitted electrons compared to the tip voltage. Spherical aberration is small because of the small ($\simeq 7°$) angular divergence of the field-emitted beam. Thus, the achievable spot size at the screen is calculated at 0.005 cm diameter if the lens can be operated at a voltage a factor of 20 higher than the tip voltage [38]. In practice, we were limited by lens breakdown to voltage ratios near 7, requiring a larger tip–lens distance, increasing the aberrations, and giving a focus diameter of $\simeq 0.03$ cm.

Although the current density (current/area) is enormous near the tip, space charge broadening of the electron beam is insignificant, because the total 10^{-5}-A current is small, and the beam is accelerated to a high velocity, reducing the charge density. The standard theory for space charge defocusing [46], which accounts for trajectory deflection by an averaged continuous charge density, predicts significant beam defocusing only for currents $\gtrsim 10^{-4}$ A.

It might be expected that, to obtain the desired time resolution with good beam focus, the deflecting field length or voltage amplitude could simply be increased to change the rate of deflection, but there is a limit to this approach. For a very fast sweeping beam, even electrons which reach the detector with zero net deflection at the middle of the sweep are deflected first in one direction, then the other, when the deflecting field reverses direction as the electrons pass through the electrodes, resulting in a wide S-shaped trajectory. To allow this wide amplitude deflection within the plates, the separation must be increased, thus reducing the net deflection with a given applied voltage.

Even if a perfectly sharp beam focus is achieved, time resolution is limited if electrons emitted over a spread of times are focused to the same spot. Since the conversion from temporal to spatial information occurs at the deflection field, such a spread is created when the time of flight (TOF) between the tip and deflecting field is not constant. One source of TOF spreading is the range of trajectories through the deflection lens followed by electrons emitted at various off-axis angles. (The theorem which guarantees the same TOF for all light rays focusing to a spot is inapplicable to particle optics.)

Another source of TOF spreading is the $\simeq 0.5$-eV spread in the distribution of energy E of the emitted electrons, given by the product of the Fermi–Dirac function with the energy-dependent tunneling probability [12]. The faster higher-energy electrons, which reach the deflecting field earliest, are deflected less by an increasing field and appear to be emitted earlier. Denoting the flight time per unit distance (i.e., 1/velocity) by τ, $d\tau/dE \simeq E^{-3/2}$, indicating that the electron energy has the largest effect on the flight time at the very beginning of the electron trajectory, when the velocity is small. In a conventional electro-optical streak camera, this effect is reduced to $\simeq 1$ ps by placing a positively biased grid very close to the photocathode [33]. In the FFEC, the TOF spreading due to initial acceleration is minimized by the very strong 1-V/Å field at the tip, which quickly accelerates the electrons to high velocity. In this strong field, only 10^{-15} s is required to accelerate an electron from rest to a velocity corresponding to the 0.5-eV energy spread. The energy effect on the TOF over the remainder of the trajectory comes predominantly from the region between the tip and the lens, before the additional accelerating effect of the lens. At the deflecting field, the effect of the electron velocity on the ease of electron deflection has a negligible effect on the detected position.

In our present instrument, we estimate a TOF flight spread of 0.3 ps from the distribution of electron trajectories, 0.090 ps from the velocity spread before the lens, and 0.050 ps from the velocity spread from the front of the lens to the deflecting plates, resulting in a net time resolution of 0.3 ps [32]. To achieve the 10^{-14}-s ultimate resolution essentially dictated by the 10^{14}-electrons/s current, the instrument must be shrunk by a factor of 30, a size of FE optics which has already been achieved [22, 47].

- *Sensitivity*

The detection scheme used in our present version of the FFEC does not quite achieve shot-noise-limited detection of the electron beam. The electrons arriving at the detector are too dense to count, so only their local density on the screen can be recorded. Ideally this local density measurement would have the same noise as if the electrons were counted. The quantum efficiency for an incident electron being amplified and detected is probably about 60%, a number which could be improved to 90% by reducing the energy of the incident electrons [48] and applying a strong entrance field to capture escaping secondaries [49]. To avoid saturating the second MCP by depleting too much charge, the MCPs are operated at a voltage so low as to give a decreasing exponential pulse height distribution (pulse height probability vs. gain),

which decreases the signal-to-noise ratio by a factor of $1/\sqrt{2}$ [50]. This problem can be overcome by using a curved-channel MCP [51], which achieves narrow pulse height distributions at a gain low enough to avoid depleting the MCP charge.

- *Spatial resolution*

Although the FE and FIM images from the same tip have the same scale, it is not possible to compare the images directly to deduce, for example, the exact position of an adsorbed Cs atom with respect to the substrate. Unfortunately, the field desorption threshold of electropositive elements such as alkalis is below the FIM imaging voltage. Although the resolution of FE images improves to better than 1 nm with decreasing tip radius, FEM images have lower resolution than FIM because of the effect of the electron velocity component parallel to the surface [52]. The FE images also depend strongly on the local electronic structure. In cases such as the adsorption of alkalis on W, this problem can probably be solved by calibrating the FE image by imaging the field-desorbed ions [53], whose position on a detector screen can be compared to the FIM image of the tip substrate. Of course, once an atom is field-desorbed, it is not available for further FEM study, but if another adsorbed atom shows an FE pattern identical to one previously located by field evaporation, it must be in the same position.

- *Energy resolution*

The Cs jumping experiments demonstrated how the detector axis perpendicular to the sweep direction can be used to record one-dimensional spatial information. By applying a time-independent electric or magnetic field to create a velocity-dependent dispersion of deflections perpendicular to the sweep direction, the energy of the field-emitted electrons can be recorded. This information characterizes the structure of the tunneling barrier [41], and in some cases the electron energy may provide lower-noise information about adsorbate position. For example, if the energy of the emitted electron is a well-defined function of atomic position [54–56] (within the uncertainty principle), a single detected electron gives the atomic position, whereas if position-dependence of the emission rate is used to determine position, the accuracy is limited by shot noise statistics.

Discussion

Experiments involving repeated measurements of position x are limited by the uncertainty principle $\Delta x \Delta p \geq \hbar/2$ relating the root mean square uncertainty of the position and momentum p. For our best spatial resolution, $2\Delta x \simeq 0.6$ nm, Δp corresponds to a velocity uncertainty of 1 m/s, about a factor of 300 below the typical velocity of a hot (800 K) Cs atom. Thus, at the spatial resolution of the FFEC, the uncertainty principle is not a limiting factor for heavy atoms and molecules.

FFEC experiments to date are a factor of 10^6 faster than any previous observations of single-atom or molecule motion [29, 57], and another factor of 100 improvement to 10^{-14}-s resolution is feasible. Adsorption, desorption, and chemical reactions should be observable by the FFEC. Although the technique can be extended to other metal surfaces and adsorbates, it is limited to adsorbates which strongly affect the field emission. The FFEC has the advantage over pump-probe techniques that an ensemble of adsorbed species need not be prepared. On the other hand, the strong electric field in the FFEC can significantly affect the dynamics (as illustrated by the CuPc experiments), and the signal-to-noise ratio is limited if only a single sweep is analyzed. If the tip returns to the same state at the end of each sweep, it may be possible to average multiple sweeps by triggering a series of identical events by laser or electrical pulses, while still continuously recording the whole sweep.

In many cases where an ordered ensemble can be prepared, observing a single molecule continuously has no real advantage over laser pump-probe observations on an ensemble. But on metal surfaces, the efficiency of pump-probe experiments using electronic excitation is greatly reduced by quenching of the electronic state. Perhaps for this reason, no time-resolved laser measurements of nuclear position have been described on a surface, although many valuable ultrafast measurements of vibrational population and phase transients have been reported [58]. The main significance of the FFEC may be in proving the response time achievable by nanometer-scale electronic devices. The STM switch of Eigler et al. based on the motion of a single atom [59] demonstrates the remarkable potential for miniaturization. If the FFEC can observe single atoms on the subpicosecond time scale, perhaps atomic motion can be controlled on that time scale as well. In the rapidly developing field of vacuum microelectronics [60], field emitters are now used as sources of miniature electron beams in fast devices.

Acknowledgments

We are grateful to Gary Kellogg and H.-W. Fink for advice on FIM and FEM, to Bruce Hoenig for technical assistance, and to Dan Auerbach, Haj Seki, Juri Matisoo, Owen Melroy, Mike Philpott, Charlie Rettner, and many other IBM colleagues for their encouragement. The early stages of this work were partially supported by the Office of Naval Research under Contract No. N00014-88-C-0419 and the Air Force Office of Scientific Research under Contract Number F49620-89-C-0068. H. H. thanks the Swiss National Science Foundation and the Treubelfonds, Basel, Switzerland, for fellowships.

References

1. J. Hirschfelder, H. Eyring, and B. Topley, *J. Chem. Phys.* **4,** 171 (1936).
2. R. D. Levine and R. B. Bernstein, *Molecular Reaction Dynamics and Chemical Reactivity*, Oxford, New York, 1987.
3. M. J. Rosker, F. W. Wise, and C. L. Tang, *Phys. Rev. Lett.* **57,** 321 (1986); Y.-X. Yan, E. B. Gamble, Jr., and K. A. Nelson, *J. Chem. Phys.* **83,** 5391 (1985).
4. For a review, see A. H. Zewail, *J. Phys. Chem.* **97,** 12,447 (1993).
5. L. Dhar, J. T. Fourkas, and K. A. Nelson, *Opt. Lett.* **19,** 643 (1994).
6. H. E. Elsayed-Ali and G. A. Mourou, *Appl. Phys. Lett.* **52,** 103 (1988); J. W. Herman and H. E. Elsayed-Ali, *Phys. Rev. Lett.* **68,** 2952 (1992); M. Dantus, S. B. Kim, J. C. Williamson, and A. H. Zewail, *J. Phys. Chem.* **98,** 2782 (1994).
7. E. L. Wolf, *Principles of Electron Tunneling Spectroscopy*, Oxford, New York, 1985; D. J. Flood, *J. Chem. Phys.* **52,** 1355 (1970).
8. C. R. Leavens and G. C. Aers, in *Scanning Tunneling Microscopy III*, R. Wiesendanger and H.-J. Güntherodt, Eds., Springer-Verlag, Berlin, 1993.
9. R. J. Hamers and D. G. Cahill, *J. Vac. Sci. Technol. B* **9,** 514 (1991).
10. S. Weiss, D. F. Ogletree, D. Botkin, M. Salmeron, and D. S. Chemla, *Appl. Phys. Lett.* **63,** 2567 (1993); G. Nunes, Jr. and M. R. Freeman, *Science* **262,** 1029 (1993).
11. A. S. Hou, F. Ho, and D. M. Bloom, *Electron. Lett.* **28,** 2302 (1992).
12. R. Gomer, *Field Emission and Field Ionization*, Harvard University Press, Cambridge, MA, 1961.
13. R. Young, J. Ward, and F. Scire, *Rev. Sci. Instr.* **43,** 999 (1972).
14. H.-W. Fink, *Phys. Scripta* **38,** 260 (1988).
15. H.-W. Fink, *IBM J. Res. Develop.* **30,** 460 (1986); H. U. Müller, B. Völkel, M. Hoffman, Ch. Wöll, and M. Grunze, *Ultramicrosc.* **50,** 57 (1993).
16. Y. Kuk and P. J. Silverman, *Appl. Phys. Lett.* **48,** 1597 (1986).
17. T. Hashizume, Y. Hasegawa, I. Kamiya, T. Ide, I. Sumita, S. Hyodo, T. Sakurai, H. Tochihara, M. Kubota, and Y. Murara, *J. Vac. Sci. Technol. A* **8,** 233 (1990.)
18. Th. Michely, K. H. Besocke, and M. Teske, *J. Microsc.* **152,** 77 (1988).
19. Vu Thien Binh and J. Marien, *Surf. Sci.* **202,** L539 (1988); Vu Thien Binh, *J. Microsc.* **152,** 355 (1988).
20. T. S. Ravi, R. B. Marcus, and D. Liu, *J. Vac. Sci. Technol. B* **9,** 2733 (1991).
21. H.-W. Fink, *Phys. Rev. Lett.* **65,** 204 (1990); R. Morin and A. Gargani, *Phys. Rev. B* **48,** 6643 (1993).
22. T. H. P. Chang, D. P. Kern, and L. P. Muray, *J. Vac. Sci. Technol. B* **10,** 2743 (1992).
23. H. Schmid and H.-W. Fink, *Appl. Surf. Sci.* **67,** 436 (1993).
24. B. D. Terris, O. Zueger, and D. Rugar, *J. Vac. Sci. Technol. B* **11,** 2315 (1993).
25. C. J. Todd and T. N. Rhodin, *Surf. Sci.* **42,** 109 (1974).
26. Ch. Kleint and K. Möckel, *Surf. Sci.* **40,** 343 (1973); W. Schütt, H. Köster, and G. Zuther, *Surf. Sci.* **45,** 163 (1974).
27. R. Gomer and D. A. Speer, *J. Chem. Phys.* **21,** 73 (1953).
28. V. T. Binh, S. T. Purcell, G. Gardet, and N. Garcia, *Surf. Sci.* **279,** L197 (1992).
29. I. Brodie, *Surf. Sci.* **70,** 186 (1978).
30. Ch. Kleint, *Surf. Sci.* **25,** 394 (1971); J.-R. Chen and R. Gomer, *Surf. Sci.* **79,** 413 (1979).
31. G. M. McClelland, U.S. Patent 5,151,594, 1992.
32. H. Heinzelmann, F. Watanabe, and G. M. McClelland, *Phys. Rev. Lett.* **70,** 3611 (1993).
33. For a collection of recent articles, see *Proc. SPIE—Int. Soc. Opt. Eng.* **1358** (1991).
34. D. L. Barr, W. L. Brown, and D. J. Thomson, *J. de Physique* **49,** C6-177 (1988).
35. V. I. Maslov, G. N. Fursey, and A. V. Kocheryshenkov, *Colloque de Physique* **50,** C8-113 (1989).
36. F. Watanabe, G. M. McClelland, and H. Heinzelmann, *Science* **262,** 1244 (1993).
37. T. Sakurai, *Atom Probe Field Ion Microscopy and Its Applications*, Academic Press, Inc., New York, 1989.
38. M. M. El Gomati, M. Prutton, and R. Browning, *J. Phys. E* **18,** 32 (1985).
39. A. P. Janssen and J. P. Jones, *J. Phys. D* **4,** 118 (1971).
40. H. S. Kim, M. L. Yu, U. Staufer, L. P. Muray, D. P. Kern, and T. H. P. Chang, *J. Vac. Sci. Technol. B* **11,** 2327 (1993).
41. J. W. Gadzuk, *Phys. Rev. B* **1,** 2110 (1970).
42. M. S. Chung, P. H. Cutler, N. M. Miskovsky, and T. E. Sullivan, *J. Vac. Sci. Technol. B* **12,** 727 (1994).
43. P. H. Lippel, R. J. Wilson, M. D. Miller, Ch. Wöll, and S. Chiang, *Phys. Rev. Lett.* **62,** 171 (1989).
44. A. J. Melmed and W. W. Müller, *J. Chem. Phys.* **29,** 1037 (1958).
45. L. W. Swanson and L. C. Crouser, *Surf. Sci.* **23,** 1 (1970).
46. M. Szilagyi, *Electron and Ion Optics*, Plenum Publishing Co., New York, 1988.
47. G. M. Shedd, H. Schmid, and H.-W. Fink, *Ultramicrosc.* **48,** 43 (1993).
48. R. R. Goruganthu and W. G. Wilson, *Rev. Sci. Instrum.* **55,** 2030 (1984).
49. R. C. Taylor, M. C. Hettrick, and R. F. Malina, *Rev. Sci. Instrum.* **54,** 171 (1983).
50. R. W. Engstrom, *Photomultiplier Handbook*, RCA, Lancaster, PA, 1980.
51. J. G. Timothy, *Rev. Sci. Instrum.* **52,** 1131 (1981).
52. D. J. Rose, *J. Appl. Phys.* **27,** 215 (1956).
53. R. S. Chambers and G. Ehrlich, *J. Vac. Sci. Technol.* **13,** 273 (1976).
54. R. Morin and H.-W. Fink, *Appl. Phys. Lett.* **65,** 2362 (1994).
55. Vu Thien Binh, S. T. Purcell, N. Garcia, and J. Doglioni, *Phys. Rev. Lett.* **69,** 2527 (1992).
56. M. E. Lin, R. P. Andres, R. Reifenberger, and D. R. Huffman, *Phys. Rev. B* **47,** 7546 (1993).
57. G. Binnig, H. Fuchs, and E. Stoll, *Surf. Sci.* **169,** L295 (1986).
58. For a review, see R. R. Cavanagh, D. S. King, J. C. Stephenson, and T. F. Heinz, *J. Phys. Chem.* **97,** 786 (1993).
59. D. M. Eigler, C. P. Lutz, and W. E. Rudge, *Nature* **352,** 600 (1991).
60. I. Brodie and P. R. Schwoebel, *Proc. IEEE* **82,** 1006 (1994).

Received December 1, 1994; accepted for publication June 28, 1995

Gary M. McClelland *IBM Research Division, Almaden Research Center, San Jose, California 95120 (mcclell@almaden.ibm.com).* After receiving his Ph.D. in chemical physics at Harvard University in 1979, Dr. McClelland spent a year as a research fellow at Stanford University. He returned to Harvard University as an Assistant Professor of Chemistry. In 1985, he joined the IBM Research Division. Dr. McClelland's research interests have included intramolecular energy transfer, gas-surface dynamics, tribology, force microscopy, field emission, ultrafast dynamics, and scanning tunneling microscopy.

Harry Heinzelmann *Institute of Physics, Klingelbergstrasse 82, 4056 Basel, Switzerland (heinzelmann@ubaclu.unibas.ch).* After receiving his Ph.D. in experimental physics at the University of Basel for work on force microscopy in 1989, Dr. Heinzelmann came to the IBM Almaden Research Center as a visiting scientist. Returning to Switzerland in 1992, he worked at the IBM Zurich Research Laboratory before recently returning to the University of Basel. Dr. Heinzelmann's research activities have included scanning force and tunneling microscopy, tribology, field emission, ultrafast dynamics, biophysics, and near-field optics for scanning microscopy and spectroscopy.

Fumiya Watanabe *Department of Materials Science and Engineering, Kyushu University, 6-10-1 Hakozaki, Higashi-ku, Fukuoka 812, Japan (watanabe@zaiko0.kyushu-u.ac.jp).* Dr. Watanabe received his Ph.D. in metallurgical engineering at the University of Illinois at Urbana in 1990. After a year as a postdoctoral research assistant at the university, he spent two years as a visiting research scientist at the IBM Almaden Research Center. He has been a lecturer at Kyushu University in Japan since December 1993. Dr. Watanabe's research interests have been primarily in surface science, particularly in atomic-level dynamics at surfaces, and in the application of surface science to semiconductor processing.